

Discrete kink dynamics in hydrogen-bonded chains I: The one-component model

V. M. Karpan^{1,2}, Y. Zolotaryuk^{1,2}, P. L. Christiansen¹, and A. V. Zolotaryuk^{1,2}

¹Section of Mathematical Physics, IMM, Technical University of Denmark, DK-2800 Lyngby, Denmark

²Bogolyubov Institute for Theoretical Physics, 03143 Kyiv, Ukraine

(March 30, 2022)

We study topological solitary waves (kinks and antikinks) in a nonlinear one-dimensional Klein-Gordon chain with the on-site potential of a double-Morse type. This chain is used to describe the collective proton dynamics in quasi-one-dimensional networks of hydrogen bonds, where the on-site potential plays role of the proton potential in the hydrogen bond. The system supports a rich variety of stationary kink solutions with different symmetry properties. We study the stability and bifurcation structure of all these stationary kink states. An exactly solvable model with a piecewise “parabola-constant” approximation of the double-Morse potential is suggested and studied analytically. The dependence of the Peierls-Nabarro potential on the system parameters is studied. Discrete travelling-wave solutions of a narrow permanent profile are shown to exist, depending on the anharmonicity of the Morse potential and the cooperativity of the hydrogen bond (the coupling constant of the interaction between nearest-neighbor protons).

05.45.Yv, 05.45.-a, 05.60.Cd

I. INTRODUCTION

Hydrogen bonds (H-bonds) play a crucial role in the structure and the dynamics in a whole variety of systems ranging from ferroelectrics to biomolecules. They are of central importance in biology, when reactions are considered at molecular level. In bioenergetics, they appear even more crucial because they enable transfers of protons from one molecule to another one in networks or chains formed via hydrogen bonding [1].

More specifically, H-bonds [2] are interactions linking two molecules or ions, for example, O, N, F, and Cl atoms, or in general any pair of hydroxyl groups, which may be denoted by X, via a hydrogen ion (proton) H^+ , forming a hydrogen-bonded (HB) bridge $X-H \cdots X$ as shown schematically in Fig. 1. The ion to which the proton in this bridge (H-bond) is more tightly linked is called the hydrogen donor, whereas the other ion is the hydrogen acceptor. More precisely, the proton is coupled to each X^- ion through a pair ion-proton interaction potential of the standard type (Morse, Lennard-Jones, etc.) with an equilibrium distance r_0 , which necessarily has a finite dissociation energy as the $X \cdots H$ distance tends to infinity.

As usual, the total potential for the HB proton is of a double-well shape, but this can occur only if the motion of the heavy ions along the H-bond is appropriately constrained, so that either (i) a sufficiently strong interaction (repulsion) between the X^- ions that does not allow the ions to get closer each other a distance less or equal to $2r_0$ or (ii) a periodic substrate potential with period exceeding $2r_0$ is additionally involved. In this way, a one-dimensional network of hydrogen bonds can be formed as a *diatomic* chain of alternating heavy (ion) and light (proton) particles coupled nonlinearly (e.g., via a Morse-type potential, like in Ref. [3]), whereas the second-neighbor (ion-ion and proton-proton) interactions are involved in

the harmonic approximation. Under certain conditions on the ion-ion coupling discussed in Ref. [4], the proton in each H-bond of the HB chain can be found in two equilibrium positions separated by a potential barrier, so that the two degenerate ground states of the chain $\cdots X-H \cdots X-H \cdots X-H \cdots$ and $\cdots H-X \cdots H-X \cdots H-X \cdots$ are assumed to exist. Another important property, more specific for biological systems, is that the height of the potential barrier crucially depends on the distance between adjacent X^- ions. Using these properties as main features of HB chains, a number of one-dimensional *two-sublattice* models, whose dynamic behavior is governed by the *soliton* theory [4], has been suggested and studied extensively. These soliton-like theories are based on the well-known *cooperativity* of the hydrogen bonding, simply defined through the coupling of protons in the nearest-neighbor hydrogen bridges of the chain.

Since the HB chain is a diatomic lattice, the mechanism of hydrogen bonding involves two types of particle displacements. Let Q_n and q_n be the displacements of the heavy ion and the proton in the n th unit cell of the lattice from their equilibrium positions, at which one of the two ground states of the chain is realized, respectively. These displacements are labeled according to the sequence $\{\dots, Q_{n-1}, q_{n-1}, Q_n, q_n, Q_{n+1}, q_{n+1}, \dots\}$. Then the general and the most simple model for the proton transfers in such a diatomic chain can be given through the two-sublattice Hamiltonian, consisting of two parts [4]:

$$H = H_0 + H_{ion}. \quad (1)$$

The first part

$$H_0 = \sum_n \left[\frac{m_p}{2} \dot{q}_n^2 + \frac{K_p}{2} (q_{n+1} - q_n)^2 + \varepsilon_0 V(u_n, \rho_n) \right], \quad (2)$$

with

$$u_n = q_n - \frac{1}{2}(Q_n + Q_{n+1}) \quad \text{and} \quad \rho_n = Q_{n+1} - Q_n, \quad (3)$$

describes the proton kinetic energy, the nearest-neighbor proton-proton interaction, and the intrabond proton energy that depends on the displacements of the protons from the midpoints in the H-bonds u_n 's and the relative distances between the nearest-neighbor ions ρ_n 's, whereas the second (pure heavy-ion) part

$$H_{ion} = \sum_n \left[\frac{1}{2} M \dot{Q}_n^2 + \frac{1}{2} K_{ion} \rho_n^2 + \frac{1}{2} K_{sub} Q_n^2 \right], \quad (4)$$

describes the kinetic energy of the X^- ions, the coupling energy between the nearest-neighbor ions, and the interaction energy of the X^- ions with a possible substrate (e.g., formed by the walls of a pore crossing a membrane). Here the overdot denotes differentiation on time t . The proton and ion masses are denoted by m_p and M , respectively. Similarly, K_p , K_{ion} , and K_{sub} stand for the stiffness constants of the interaction between the nearest-neighbor protons, the nearest-neighbor ions, and the chain ions with the substrate, respectively. It is important that the intrabond proton energy is given in terms of a general double-well potential $V(u, \rho)$ as a function of two variables: u , the proton displacement from the middle of the hydrogen bond, and ρ , the relative ion displacement. If additionally this (dimensionless) function is normalized according to the relations $V(0, 0) = 1$ and $V(\pm a, 0) = 0$, where $\pm a$ are the positions of minima in this function, then ε_0 is the barrier height of the proton potential in the H-bond. When the heavy ions are displaced from their equilibria, this potential is deformed, with its barrier top moved together with the ions.

There have been numerous studies [4] of soliton solutions to the equations of motion governed by the Hamiltonian (1)-(4) including also one-component models, where the heavy ions X^- are assumed to be fixed [5–11]. All these studies refer to the continuum limit, which presumes the existence of a sufficiently effective cooperativity of hydrogen bonding or, in other words, the interbond proton-proton coupling K_p is required to be strong enough. However, according to the *ab initio* calculations of the proton-proton interaction in realistic HB chains by Godzik [12], $K_p \simeq 41$ Kcal/mol \AA^2 . This magnitude appears not to be sufficient for a *free* propagation of the ionic defects along the HB chain with realistic values of the potential barrier height ε_0 . The reduction of this barrier on the basis of the two-component modelling was also shown to be not enough to provide a free soliton regime and the ionic defects in HB chains with realistic parameter values [13] were shown to be very narrow objects [14].

On the other hand, a rapidly increasing number of publications over last years (since the pioneering work of Peyrard and Kruskal [15]) have demonstrated significant differences in the behavior of soliton solutions treated

in the continuum limit and their spatially discrete relatives [16]. The discrete versions of the partial differential equations brings about a number of critically important modifications to the dynamics. The moving kinks of the continuum theories become propagating structures that decelerate by emitting radiation as they traverse the lattice sites. This ultimately brakes the structures and brings them to rest, or “pins” them.

The above results has been obtained for the conventional models such as the discrete sine-Gordon and ϕ^4 chains. For more general class of models, some interesting and intriguing results has been obtained. Thus, it has been shown that the *shape* of the on-site (in our case, the intrabond proton energy) potential is a factor of particular importance for modelling soliton motion in physical systems. To study this effect, Peyrard and Remoissenet [17] have introduced a modified sine-Gordon system, where the shape of the on-site potential differs sufficiently from the sin-function. They found that if the barrier between the potential wells is flat enough, the Peirels-Nabarro (PN) barrier does not decrease monotonically with the coupling constant, as in the ordinary discrete sine-Gordon chain. It decreases with oscillations, so that the PN barrier experiences dips, where it lowers by the order of magnitude. Later [18], it was found that if the PN barrier decreases nonmonotonically, there exist certain velocities, at which even very discrete kinks propagate with constant shape and velocity. Everywhere in between these velocities, there exist kinks with oscillatory asymptotics (nanopterons). Approaching the problem from another side, Schmidt in [19] has constructed a Klein-Gordon model that allows an exact moving kink solution of the form $\tanh(n-vt)$ for some specific value of velocity v . Furthermore, Flach and coauthors [20] have shown that for this model the PN barrier is nonzero (when $v \neq 0$). It was also shown that kinks of the discrete sine-Gordon equation with topological charges greater then one exhibit some features, similar to those, described above, including free propagation at some selected velocities (see Refs. [15,23,18]). Note that if we step out from the Klein-Gordon class of discrete models (for instance, by introducing anharmonicity into the interparticle interaction), some new phenomena related to the kink mobility can appear, but this is out of the scope of the present paper. In this context, a few papers (see Refs. [21,22] and others therein) should also be mentioned.

Thus, owing to the importance of discreteness effects in the kink dynamics, it would be of big interest to apply these findings first for the one-component model of proton transport in HB chains and then for the two-component model given by the Hamiltonian (1)-(4). In this context, as found by Duan and Scheiner [24,25], a pair of Morse functions, placed tail-to-tail so as to allow for the approach of the proton towards the acceptor while it is departing from the donor (see Fig. 1), provides the best framework for reproducing their potentials obtained from *ab initio* calculations. It is important that

the Morse-type functions contain parameters with clear physical meaning, which vary little from one H-bond to the next one in HB systems.

The aim of this paper is to investigate the properties of the one-dimensional Klein-Gordon chain with the on-site (intrabond) potential of the double-Morse type. We are going to find both stationary and dynamic (moving) kink solutions and to show that kinks can be mobile even if being very narrow.

The paper is organized as follows. In the next section, we present the Hamiltonian and the equations of motion for the one-component model. In Sec. III, we study the properties of the stationary kink solutions. In Sec. IV, the Peierls-Nabarro potential for the kinks is investigated. Section V is devoted to the studies of kink mobility. Conclusions are given in Sec. VI.

II. THE DOUBLE-MORSE PROTON POTENTIAL

In the limit, when the heavy ions are fixed (immobile) at a same distance l forming a uniform lattice, we deal only with the first part of the Hamiltonian (2), where $q_n = u_n$. In what follows we adopt the dimensionless description, where for the dimensionless proton displacement u_n/l we keep the same notation u_n and use the time unit $t_0 = l/\sqrt{\varepsilon_0/m_p}$. In these dimensionless variables, the Hamiltonian (2) reads

$$\mathcal{H} = \sum_n \left[\frac{1}{2} \dot{u}_n^2 + \frac{\kappa}{2} (u_{n+1} - u_n)^2 + V(u_n) \right]. \quad (5)$$

Here and in what follows, the overdot denotes the differentiation with respect to $\tau = t/t_0$ and $\kappa = K_p l^2/\varepsilon_0$ is the dimensionless proton-proton coupling constant.

As described in Introduction and illustrated by Fig. 1, the intrabond proton potential $V(u)$ can be formed as a result of superposition of two pair ion-proton interaction potentials placed tail-to-tail. According to the *ab initio* studies of Duan and Scheiner [24,25], these potentials are preferred to be chosen of the Morse type. As a result, the potential $V(u)$ is a symmetric double-well function with minima at $u = \pm a$ and a maximum at $u = 0$ [4,26,27]:

$$V(u) = \left[\frac{\alpha - \cosh(\beta u)}{\alpha - 1} \right]^2, \quad \alpha = \cosh(\beta a). \quad (6)$$

The inequality $\alpha > 1$ ensures the double-well form of the function (6). Throughout the paper we take $a = 0.25$. The potential (6) is normalized so that the barrier height always equals unity. Its shape for different values of β is shown in Fig. 2. As can be seen from this figure, the parameter β determines the curvature/flatness of the barrier and its shape strongly depends on this parameter. We assume its values to range over the whole half-axis $0 < \beta < \infty$. For small β , the barrier is rather narrow being the limiting case of the ϕ^4 model, i.e.,

$$\lim_{\beta \rightarrow 0} V(u) = (1 - u^2/a^2)^2. \quad (7)$$

Increase of β makes the barrier more flat and the wells more narrow, so that the other limit is

$$\lim_{\beta \rightarrow \infty} V(u) = \begin{cases} \infty, & -\infty < u < -a, \\ 0, & u = \pm a, \\ 1, & -a < u < a, \\ \infty, & a < u < \infty. \end{cases} \quad (8)$$

The corresponding equation of motion is the well known discrete nonlinear Klein-Gordon equation:

$$\ddot{u}_n = \kappa (u_{n+1} - 2u_n + u_{n-1}) - V'(u_n), \quad n = 0, \pm 1, \dots \quad (9)$$

Here and in what follows the prime denotes differentiation of a function with respect to its argument.

Before embarking on a complete analysis of the discrete equation (9), we calculate the dispersion law of small-amplitude waves around one of the two ground states. As a result, this law is given by the following equation:

$$\begin{aligned} \omega^2(q) &= \omega_0^2 + 2\kappa(1 - \cos q), \\ \omega_0 &= \sqrt{2 \frac{\alpha + 1}{\alpha - 1}} \beta = \frac{\sqrt{2}\beta}{\tanh(\beta a/2)}. \end{aligned} \quad (10)$$

The gap of the spectrum depends on the parameter β ; for large values of β , it increases linearly with β .

III. KINK STATES, THEIR STABILITY AND BIFURCATIONS

In this section, we start from the classification of possible stationary (anti)kink states. To compute these states, we have used both the conjugate gradients method for minimization of the stationary part ($\dot{u}_n \equiv 0$) in the Hamiltonian (5) and the Newton iteration method for solving the time independent nonlinear set of equations that originates from Eqs. (9):

$$\kappa(u_{n+1} - 2u_n + u_{n-1}) = V'(u_n), \quad n = 0, \pm 1, \dots \quad (11)$$

These equations can be rewritten as a two-dimensional map:

$$\begin{aligned} p_{n+1} &= u_n, \\ u_{n+1} &= \kappa^{-1} V'(u_n) + 2u_n - p_n, \quad n = 0, 1, \dots \end{aligned} \quad (12)$$

In general, maps of this type are chaotic. However, an on-site potential, for which the map (12) is integrable, has been found in Ref. [28]. The previous knowledge on the kink solutions in the most popular cases of the discrete nonlinear Klein-Gordon lattices such as the sine-Gordon or ϕ^4 chains implies the existence of only two stationary kink states. These states possess the inversion symmetry with respect to the center of the kink, being monotonic

functions on the lattice. They connect two hyperbolic fixed points of the map $(-a, -a)$ and (a, a) , which are the ground states of the chain.

Adapted to our case of a HB chain with the numbering of ions and protons according to the sequence $\{\dots, Q_{n-1}, q_{n-1}, Q_n, q_n, Q_{n+1}, q_{n+1}, \dots\}$, one of these stationary states, which has its center positioned at a heavy ion (call it an ion-centered kink/antikink), say with a number n_0 , is dynamically *stable*, whereas the other, with its center positioned in the middle of a n_0 th H-bond, i.e., in between the n_0 th and the $(n_0 + 1)$ th ions (call it a bond- or proton-centered kink/antikink), is dynamically *unstable*. The symmetry of the ion-centered (on the n_0 th ion, in between H-bonds $n_0 - 1$ and n_0) kink/antikink is defined by the relations

$$u_{n_0-n} = -u_{n_0+n-1}, \quad n = 0, \pm 1, \dots, \quad (13)$$

whereas for the proton-centered (in the middle of the n_0 th H-bond, in between ions n_0 and $n_0 + 1$) kink/antikink, the symmetry relation is given by

$$u_{n_0-n} = -u_{n_0+n}, \quad n = 0, \pm 1, \dots \quad (14)$$

The solutions of these types certainly exist also in our model, as illustrated by Fig. 3. However, their stability properties appear to be much more complicated and they are discussed below.

In general, a deformation of the barrier shape in the potential $V(u)$ leads to a more rich family of kink/antikink solutions. This has been observed in the previous studies [17,18]. The first feature caused by the deformation of the proton potential (6) with increase of β is the phenomenon of *stability switching*, according to which the two types of kink solutions with inversion symmetry defined by Eqs. (13) and (14) switch their stability, while varying the system parameters. The second one is the appearance of new types of kink solutions. For the first of these types the symmetry relations (13) and (14) are not valid anymore, whereas the other one is symmetric with a zigzag-like profile at their center, but still has monotonic asymptotics as $|n| \rightarrow \infty$.

A. An exactly solvable limit

To understand better the effect of stability switching, it is instructive to consider the limit $\beta \rightarrow \infty$, resulting in a similar potential behavior as studied in Ref. [18]. In this limit, the double-Morse potential takes the form [see Eq. (8)], for which the system of equations of motion (11) becomes exactly solvable because the particles (protons) can appear only either in the wells or on the flat region of the proton potential $V(u)$. There exists an infinite, but a countable set of the stationary kink solutions with an arbitrary number of particles, $m = 0, 1, \dots$, lying on the barrier. This number uniquely defines a kink/antikink solution. The set of these solutions can be written as

$$u_n = \begin{cases} -a, & -\infty < n \leq n_0 - \frac{m}{2} - 1, \\ 2a \frac{n-n_0+1/2}{m+1}, & n_0 - \frac{m}{2} - 1 < n < n_0 + \frac{m}{2}, \\ a, & n_0 + \frac{m}{2} \leq n < \infty, \end{cases} \quad (15)$$

for the kink centered on the n_0 th ion ($m = 0, 2, \dots$) and

$$u_n = \begin{cases} -a, & -\infty < n \leq n_0 - \frac{m+1}{2}, \\ 2a \frac{n-n_0}{m+1}, & n_0 - \frac{m+1}{2} < n < n_0 + \frac{m+1}{2}, \\ a, & n_0 + \frac{m+1}{2} \leq n < \infty, \end{cases} \quad (16)$$

for the kink centered on the n_0 th H-bond ($m = 1, 3, \dots$). Similarly, the analytical expressions for the antikink solutions can be obtained. These stationary solutions can be found, using either energy arguments based on the Hamiltonian (5) or directly from the equations of motion (11), where

$$\lim_{\beta \rightarrow \infty} V'(u) = \begin{cases} -\infty, & -\infty < u < -a, \\ 0, & -a \leq u \leq a, \\ \infty, & a < u < \infty. \end{cases} \quad (17)$$

The energy of both these (anti)kink solutions in the limit $\beta \rightarrow \infty$ is easily calculated and for any integer $m = 0, 1, \dots$, it reads

$$E_m = E_m(\kappa) = m + 2\kappa a^2 / (m + 1). \quad (18)$$

As illustrated by Fig. 4, where the linear dependences of the energy E_m on κ are plotted for different m 's that the crossings of these dependencies occur at some values of the coupling parameter κ .

The most interesting points in Fig. 4 are the crossings for the states with the energies that correspond to adjacent m 's, i.e., $m = 0$ and 1 , $m = 1$ and 2 , and so on because they occur at lowest energies. Thus, the crossings when the kink state with m particles on the barrier is transformed into the state with $m + 1$ particles on it, occur at the following values of κ :

$$\kappa_{m+1}^{(c)} = (m + 1)(m + 2) / 2a^2, \quad m = 0, 1, \dots \quad (19)$$

Therefore, depending on the strength of the proton-proton coupling κ , the proton-centered or the ion-centered kink can reach a global minimum of the energy $E_m > 0$ (except for the ground states, when $E = 0$). In addition, it is interesting to notice that at the values of κ given by Eqs. (19), the inter-bond and the intrabond energies are equal exactly each other.

B. Numerical results for finite β 's

Now let us investigate how the properties of the kink solutions found in the exactly solvable limit $\beta \rightarrow \infty$ change, when β take finite values. Thus, changing β allows us to explore the whole set of scenarios, starting from the ϕ^4 limit and finishing with the limit $\beta \rightarrow \infty$.

We start to compute the kink solutions from the anticontinuous limit ($\kappa = 0$), taking the solutions of the exactly solvable limit as an initial guess for the Newton iteration method. Then, we increase κ and check how the kink profiles behave. In Fig. 5, the energy dependence on the coupling parameter κ is plotted for $\beta = 10$. First, let us focus on the behavior of the solutions with the lowest energies (namely those which correspond to $m = 0$ and $m = 1$ in the exactly solvable limit).

In Fig. 5, curve 1 corresponds to the ion-centered kink with $m = 0$, the symmetry of which is given by Eqs. (13), whereas curve 2 to the proton-centered kink with $m = 1$, the symmetry of which is given by Eqs. (14). Contrary to the previous knowledge on the stability properties of the kink solutions for the discrete sine-Gordon and ϕ^4 models, where the (anti)kinks of the symmetry (13) are always dynamically stable, while the (anti)kinks of the symmetry (14) are always dynamically unstable, an interchange of stability is observed for the proton potential (6) with finite β 's as κ varies. Thus, one can see that at a certain value of the coupling parameter, $\kappa \simeq 24.5$, the energies of the both types of symmetric kinks coincide and after passing this critical point, the proton-centered kink appears to be stable, while the ion-centered kink is unstable. For higher κ 's, several more interchanges of stability take place, with the energy difference between the sequential kink states that decreases with the growth of κ . These transitions of stability take place smoothly all the way up to the continuum limit. We refer to these transitions as to *stability switchings*. Thus, the solutions with $m > 1$, which were clearly separated from the $m = 0$ and the $m = 1$ solutions in the exactly solvable limit $\beta \rightarrow \infty$, appear to be smoothly connected with them. In other words, while the coupling κ increases, the particles slowly “climb” on the barrier, so that there is no abrupt transition from the state with $m = 0$ to the state with $m = 2$ or, further, to the states with $m = 4, 6, \dots$. The same can be concluded about the kinks with m being odd. In this respect, the system still shows similarity with the ϕ^4 model.

If we focus more carefully on the behavior of the system in the vicinity of the points, where the energies of proton-centered and ion-centered kinks become equal, we find that a new type of kinks appears. These kinks shown in Fig. 6 do not exhibit any of the symmetries defined by Eqs. (13) and (14), but they are doubly degenerate related to each other by the inversion with respect to the crossing point between the line $u_n = 0$ and the line connecting two central particles of the kink [$n = 48$ and $n = 49$ in Fig. 6(a)]. The energy of these kink states with broken symmetry is always larger than the energy of the symmetric (ion-centered and proton-centered) kinks. The asymmetric (anti)kinks are always linearly unstable. In Fig. 5, their energy is shown by curve 3.

The kinks of the last type are shown in Fig. 5 by curves 4 and 5. This is what happens to the solutions with $m > 1$ obtained in the limit $\beta \rightarrow \infty$, when we are moving from the anticontinuous limit ($\kappa = 0$). Instead of attaining a

regular monotonic form, the kink profiles with several particles on the barrier develop a zigzag-like structure in their centers, as demonstrated by Fig. 7. For finite β 's the zigzag-like solutions are linearly unstable and therefore we do not study them here in more detail.

Instead, we focus on the behavior of the *monotonic* kink solutions with increase of the coupling κ in the vicinity of the stability switchings. To understand this effect better, in Fig. 8, we have plotted the position of the $(N/2)$ th proton (N is the total number of H-bonds in the chain) as a function of the coupling κ . Here the sequence of pitchfork bifurcations is clearly seen. Curve 1 corresponds to the kink centered in the middle of the $(N/2)$ th bond, i.e., when the $(N/2)$ th proton is always a central particle of the kink with $u_{N/2} \equiv 0$. The displacements of the $(N/2)$ th proton for the ion-centered kinks positioned on the $(N/2 + 1)$ th and the $(N/2)$ th ions are shown by curves 2 and 3, respectively. When increasing κ , the $(N/2)$ th proton moves slowly out of the well. At a certain value of κ , more specifically, at $\kappa \simeq 22.5$, the pitchfork bifurcation of the proton-centered kink takes place. This configuration retains its stability and two new solutions (both linearly unstable) appear. These are precisely those asymmetric kinks (see curves 4 and 5 in Fig. 8), with their shape shown in Fig. 6. At the beginning, they look like slightly distorted proton-centered kinks, but with the growth of κ , they change more and more towards the ion-centered configuration. Eventually, the second pitchfork bifurcation takes place at $\kappa \simeq 26.2$. The asymmetric kinks join the ion-centered kinks (junction of curves 3 and 4, and curves 2 and 5) and the ion-centered configuration loses its stability. Now one can clearly see that two identical kinks, shifted by one lattice spacing with respect to each other, are connected via such a bifurcation sequence. Thus, this pitchfork bifurcation is nothing but a transition of the kink from one position to another position, one lattice period forward or backwards. This cascade of bifurcations can be continued further up or down in u_n 's or, in other words, two or more sites backwards or forward. Similar bifurcation scenario for discrete breathers in the ac-driven and damped Klein-Gordon lattice has been reported in [29].

For higher values of β , the effect of stability switchings exists, being more pronounced because the switchings start at smaller κ and take place more frequently (see Fig. 9). Another feature that appears from the exactly solvable limit $\beta \rightarrow \infty$ is as follows. Curve 1 of Fig. 9 corresponds to the ion-centered kink and curve 2 to the proton-centered kink. They cross each other at $\kappa \simeq 17.4$, where the ion-centered kink loses its stability, disappearing shortly at $\kappa \simeq 28.6$. Here the same pitchfork bifurcation scenario takes place, but the distance between the first and the second bifurcations is much larger than in the $\beta = 10$ case. In the meanwhile, a bit earlier, at $\kappa \simeq 23.4$, a new family of ion-centered kinks appears (curve 4). This curve corresponds to the ion-centered kinks with two protons on the barrier. Thus, one can observe the coexistence of two different kink solutions

with the same type of symmetry (for more details see the upper inset of Fig. 9). This coexistence takes place on a rather narrow interval of κ and one of the coexisting kinks is unstable, but still this phenomenon clearly originates from the limit $\beta \rightarrow \infty$. In Fig. 10, we show the shape of two coexisting kinks. One of them (more narrow) corresponds to curve 1 of Fig. 9 and the second one, which is more broad, corresponds to curve 4 of this figure. These kinks have zero and two protons on the barrier, respectively. When κ increases further, the stability switchings occur between curves 2 and 4 under the same scenario as before for $\beta = 10$ (see for details the lower inset of Fig. 9). Zigzag-like kinks are also presented in this case, as shown by curves from 6 to 8.

When increasing β even more, the coexistence of different kinks with the same symmetry is even more pronounced. We have checked the case of $\beta = 50$ and discovered for this value that several cases of this coexistence for different kinks take place and they are much more pronounced. Thus, this case is rather close to the exactly solvable limit $\beta \rightarrow \infty$.

C. Analytical approximation for finding kink solutions

One can use a simplification of the potential (6) in order to obtain analytically an exact (anti)kink solution. To this end, we approximate both the wells of the potential by parabolas connected by the constant equal to the barrier height as follows:

$$V(u) \simeq \begin{cases} (\omega_0^2/2)(u+a)^2, & -\infty < u < -b, \\ 1, & -b \leq u \leq b, \\ (\omega_0^2/2)(u-a)^2, & b < u < \infty, \end{cases} \quad (20)$$

where $b = a - \sqrt{2}/\omega_0$. Schematic description of this “parabola-constant” approximation is presented in Fig. 11 by thick solid lines. The thin solid lines show the original potential (6) with $\beta = 20$. The approximation is expected to work well, when the barrier is flat enough, i.e., when $\omega_0 \gg \sqrt{2}/a$. Within this approximation, we are able to solve the problem of finding stationary kink solutions analytically.

Let $m = 0, 1, \dots$, be the number of protons on the barrier of the potential (20). Then the discrete kink profiles are given by

$$u_n = \begin{cases} -a + A_m e^{\lambda(n-n_0+m/2+1)} & \text{if } -\infty < n \leq n_0 - m/2 - 1, \\ (n - n_0 + 1/2)D_m & \text{if } n_0 - m/2 - 1 < n < n_0 + m/2, \\ a - A_m e^{-\lambda(n-n_0-m/2)} & \text{if } n_0 + m/2 \leq n < \infty, \end{cases} \quad (21)$$

for the kink centered on the n_0 th ion ($m = 0, 2, \dots$) and

$$u_n = \begin{cases} -a + A_m e^{\lambda[n-n_0+(m+1)/2]} & \text{if } -\infty < n \leq n_0 - (m+1)/2, \\ (n - n_0)D_m & \text{if } n_0 - (m+1)/2 < n < n_0 + (m+1)/2, \\ a - A_m e^{-\lambda[n-n_0-(m+1)/2]} & \text{if } n_0 + (m+1)/2 \leq n < \infty, \end{cases} \quad (22)$$

for the kink solution centered on the n_0 th H-bond ($m = 1, 3, \dots$). Here λ is a “localization” parameter that measures the transition width in the (anti)kink profile between the uniform distribution of protons on the barrier and the (anti)kink asymptotics $u_n \rightarrow \pm a$. It is given by a positive root of the equation

$$\cosh \lambda = 1 + \omega_0^2/2\kappa. \quad (23)$$

The other two parameters, the amplitude A and the uniform distance between the nearest-neighbor protons on the flat D can be expressed through the localization parameter λ as

$$A_m = \frac{2a}{(m+1)e^\lambda - m + 1}, \quad D_m = \frac{2ae^\lambda}{(m+1)e^\lambda - m + 1}. \quad (24)$$

As follows from Eqs. (10) and (23), the limit $\lambda \rightarrow \infty$ (when $\omega_0^2/\kappa \rightarrow \infty$) is more general than the limit $\beta \rightarrow \infty$ because λ contains both β and κ . Therefore one can check that Eqs. (21)-(24) are reduced to the stationary kink solution given by Eqs. (15) and (16) as $\lambda \rightarrow \infty$. In particular, the amplitude A_m and distance between the protons on the barrier D_m tend to zero and $2a/(m+1)$, respectively.

Using Eqs. (21)-(24) one can easily compute the energy of both the kink configurations:

$$E_m = m + 2\kappa a^2 \frac{\tanh(\lambda/2)}{1 + m \tanh(\lambda/2)}. \quad (25)$$

Similarly, this expression is also transformed to the energy (18) as $\lambda \rightarrow \infty$.

Now we investigate the behavior of the energy difference

$$\Delta E_{m+1}(\kappa, \beta) = E_{m+1} - E_m, \quad m = 0, 1, \dots \quad (26)$$

We find that this difference as a function of κ has a number of zeroes and these zeroes depend on the parameter β . Thus, within our approximation one can predict the effect of switching of the stable and unstable kink configurations. In Table I, we show the values of the coupling parameter κ , for which the first [i.e., when $\kappa = \kappa_1$ and $m = 0$; see also Eq. (19)] switching of the kink stability takes place.

TABLE I. Comparison of numerically and analytically calculated values of κ for which the first ($m = 0$) stability switching occurs.

β	κ_1 , numerical	κ_1 , analytical
5	64.10	18.0
10	24.547	17.069
20	17.383	16.329
50	16.172	16.052
∞	16.0	16.0

We see that the approximation works fairly well when β is rather large and the barrier between the wells is close to being completely flat. It is improving with increase of β and in the limit $\beta \rightarrow \infty$, our approximation coincides with the exact result, shown above. Thus, switchings of the stability of kink states with different symmetries is a generic effect that does not depend on a specific model, but on the properties of the on-site potential. Another piecewise approximation of the proton potential $V(u)$ for a HB chain has been constructed earlier by Weiner and Askar [30], using alternatively inversed parabolas. Our potential approximation (20) seems to be more appropriate for the studies in detail of flatness effects of the on-site (intrabond) potential and more close to the realistic double-Morse potential (6) if β is not so small.

Note that the zigzag-like kink profiles obtained above numerically shown, e.g., in Fig. 7 can also be given analytically within the approximation (20). Indeed, the ion-centered kink shown in Fig. 7(a) is described by

$$u_n = \begin{cases} -a + B_0 e^{\lambda(n+2)}, & n = -2, -3, \dots, \\ u_0 = -u_{-1} = \xi_0, & \\ a - B_0 e^{-\lambda(n-1)}, & n = 1, 2, \dots, \end{cases} \quad (27)$$

whereas the proton-centered profile illustrated by Fig. 7(b) is given by

$$u_n = \begin{cases} -a + B_1 e^{\lambda(n+2)}, & n = -2, -3, \dots, \\ u_0 = 0, \quad u_1 = -u_{-1} = \xi_1, & \\ a - B_1 e^{-\lambda(n-1)}, & n = 1, 2, \dots, \end{cases} \quad (28)$$

where λ is given by Eq. (23) and

$$B_m = 2a \frac{e^\lambda + e^{-\lambda} - m/2 - 1}{e^\lambda (e^\lambda - m + 1)},$$

$$\xi_m = a \frac{3 - e^\lambda - 2e^{-\lambda}}{e^\lambda - m + 1}, \quad m = 0, 1. \quad (29)$$

Using the last equations, the kink energy can be calculated in a similar way as the energy (18). In the limit $\lambda \rightarrow \infty$, the energy of the zigzag-like kinks, profiles of which are illustrated by Fig. 7, become

$$E_0 = 6\kappa a^2 \quad \text{and} \quad E_1 = 1 + 5\kappa a^2. \quad (30)$$

These expressions clearly show that for this type of kinks their energies also can coincide for certain values of coupling κ if β (and, consequently, λ) is large enough.

D. Elementary excitations on the kink background

Let $u_n^{(0)}$ be a stationary kink solution of Eq. (11), i.e., a fixed point of the map (12). We are interested in the properties of small-amplitude excitations on the kink background. Linearizing Eq. (9) around the stationary kink solution according to

$$u_n = u_n^{(0)} + A_n e^{i\Omega\tau}, \quad (31)$$

we arrive at the eigenvalue problem

$$\hat{L}\mathbf{A} = \Lambda\mathbf{A}, \quad \mathbf{A} = \{\dots, A_{n-1}, A_n, A_{n+1}, \dots\}. \quad (32)$$

Here the operator \hat{L} [the Hessian of the Hamiltonian Eq. (5)] acts on a vector \mathbf{A} as

$$(\hat{L}\mathbf{A})_n = -\kappa(A_{n+1} - 2A_n + A_{n-1}) + V_n A_n, \quad (33)$$

where $V_n = V''[u_n^{(0)}]$. The operator \hat{L} is a symmetric (so all eigenvalues are real) tridiagonal matrix and the spectral parameter is $\Lambda \equiv \Omega^2$. This eigenvalue problem can be treated as a quantum-mechanical problem of a particle, trapped in a single-well spatially discrete potential formed by the kink. Its depth depends on the curvature/flatness of the proton potential in the middle of the H-bond, $V''(0)$, and tends to ω_0^2 as $n \rightarrow \pm\infty$.

The eigenvalues of the problem also give information about the linear stability of the kink solution. If there exists at least one eigenvalue $\Lambda = \Omega^2 < 0$, the linear excitation on the kink grows exponentially in time and the corresponding kink solution is linearly unstable. Otherwise, it is linearly stable. The stability of stationary kink solutions is determined by the system parameters (in our case, by the curvature/flatness parameter β and the coupling κ).

In Fig. 12, we depict the dependence of the eigenfrequencies Ω_n 's on the coupling parameter κ for different curvatures β . The spectrum consists of two parts. The first one describes the eigenfrequencies that lie above the potential V_n and therefore determine delocalized eigenvectors corresponding to the linear (phonon) spectrum of the lattice. The second part consists of eigenfrequencies that lie below ω_0^2 corresponding to spatially localized eigenvectors. The lowest eigenfrequency is the Goldstone mode, which is universally presented in all the Klein-Gordon models.

The second mode corresponds to small-amplitude oscillations of the kink core, being often referred to as the Rice mode. In the continuum ϕ^4 model, there are only two localized modes: the Goldstone mode and the Rice mode. The properties of the internal modes can be significantly altered due to different factors such as change of the nature of the interparticle interaction [31] or change of the shape of the on-site potential [32]. If β is not so large, the behavior of the eigenfrequencies and eigenvectors (see Fig. 13) of our system is reminiscent to that of the ϕ^4 model, as shown in panels (a) and (b) of Fig. 12. However, several differences occur. Thus, the Goldstone mode collides with the zero axis and becomes unstable [see Fig. 12(a)] for the ion-centered kink. Meanwhile, for the proton-centered kink [see Fig. 12(b)], the Goldstone mode was initially unstable and became stable later on. The stability switchings are caused by the pitchfork bifurcations as described at the beginning of this section. Another difference is the appearance of the new eigenfrequency for the proton-centered kink with the eigenvector which has two nodes [see Fig. 13(e)].

Thus, one can see that curvatures play an important role in the properties of the eigenfrequencies of our system. Increasing β further, we observe more pitchfork bifurcations of the Goldstone mode and the appearance of more localized modes. In panels (c) and (d), we show how the eigenfrequencies behave for $\beta = 10$. We observe more localized internal modes, some of them surviving in the continuum limit and some of them disappearing there. The shape of the corresponding eigenvectors (see Fig. 14) behaves accordingly to the wavefunction shape of the bound states of the quantum-mechanical Schrödinger equation.

IV. PROPERTIES OF THE PEIERLS-NABARRO BARRIER

In general, the propagation of topological solitons (kinks and antikinks) in lattices are subject to their discreteness. The discreteness effects can be described by a spatially periodic potential with the period coinciding with the lattice spacing l , known as a Peierls-Nabarro (PN) potential. The PN potential $E_{PN}(n_c)$ is a function of the kink center position

$$n_c = \sum_n n \frac{u_{n+1} - u_{n-1}}{2(u_\infty - u_{-\infty})} = \frac{1}{4a} \sum_n n(u_{n+1} - u_{n-1}), \quad (34)$$

and the height of the PN barrier equals

$$\delta E = E(n_{c,max}) - E(n_{c,min}). \quad (35)$$

This difference measures the activation energy for the kink propagation though one lattice spacing. Here $n_{c,max}$ and $n_{c,min}$ are the positions of the kink, where the PN potential has its maxima or minima, respectively. The minimum position $n_{c,min}$ coincides with the kink position, which is a global minimum of the kink energy. Thus, normally $n_{c,min}$ is an integer or a half-integer.

It is a well established fact that for the ϕ^4 and sine-Gordon models, the height of the PN barrier coincides with the difference between the energies of the proton-centered and ion-centered kinks. As demonstrated above, the deformation of the proton (intrabond) potential $V(u)$ leads to the switching of stability of these two states. This does not mean, however, that the PN barrier disappears, when the energy of these states coincides because the site-centered and proton-centered states do not represent the states with the highest and the lowest energy of the PN potential [17,18,32].

In Fig. 15, some examples of variation of the energy $E(n_c)$ for different values of κ are presented. Panel (a) corresponds to the situation, when the proton-centered kink is an energy minimum and the ion-centered one reaches a maximum. The second panel (b) demonstrates the case, when the first pitchfork bifurcation occurs and the asymmetric kink appears. Panel (c) corresponds to

the case, when the stability switching happens and both the proton- and ion-centered kink states get minima, and the asymmetric kinks are maxima. The period of the PN potential is decreased by one half. After that, as shown in panel (d), the proton-centered kink becomes unstable and the ion-centered one stable. The last panel (e) is obtained after the second pitchfork bifurcation has occurred and the asymmetric kinks disappear.

Dependence of the PN barrier is non-monotonic not only in κ but also on β . In Fig. 16, we show the dependence of the PN barrier on the parameter β for a fixed value of κ . We observe a minimum at $\beta \simeq 8.3$, which is obviously caused by the stability switching. Indeed, as shown by the upper inset, the minimum of the PN potential moves from a half-integer value to an integer one. Thus, the stable kink configuration changes from the ion-centered to the proton-centered kink. Note, that the height of the PN barrier does not attain zero (see the lower inset), but decreases by two order of magnitude.

V. DISCRETE KINK MOBILITY

Another interesting consequence of the deformation of the on-site potential barrier is the possibility of the existence of non-oscillating travelling kinks. In the continuum Klein-Gordon models which admit moving topological solitons (kinks and antikinks), the domain of admissible soliton velocities s is the interval $0 \leq s < c_0$, where $c_0 = \sqrt{\kappa}$ is the characteristic velocity. Thus, kinks in these continuum models are a one-parametric family of solutions with the kink velocity s as a parameter. In a general case of the discrete Klein-Gordon model, this family is reduced to a *discrete* set of travelling kink solutions with some velocities s_0, s_1, \dots, s_k , $s_0 = 0$, $s_k < c_0$. In the ϕ^4 and the sine-Gordon models, there exists only s_0 . In general, everywhere in between s_n 's, there exist moving kinks with *oscillating* asymptotics known as *nanopterons*. The existence of velocities $s_n \neq 0$ has been shown both numerically [18] and analytically [19,20] for several models. This effect is due to the properties of the on-site (intrabond) potential $V(u)$ and, more precisely, the flatness of its barrier which, in its turn, causes the stability switchings described in the previous sections.

For finding non-oscillating kink solutions, we have used a pseudospectral method [33]. The method allows us to find the travelling-wave kink solutions of the type

$$u_n(t) = u(n - s\tau) \equiv u(z), \quad (36)$$

solving the differential equation with advanced and delay terms:

$$s^2 u''(z) = \kappa [u(z+1) - 2u(z) + u(z-1)] - V'[u(z)]. \quad (37)$$

Dependence of the kink velocity on the coupling parameter κ is shown in Fig. 17. As follows from this figure,

it starts (see curve 1) at the value of κ , which is close to that when the pitchfork bifurcation takes place (see Fig. 8). Then the velocity grows with κ . The second velocity dependence starts at κ being close to the point of the second pitchfork bifurcation.

Dependence of the kink velocity on the parameter β has similar behavior, as demonstrated by Fig. 18. It is interesting to note that the value of the velocity of the moving kink does not decrease down to zero as κ or β decreases, but stops at some finite s instead. This means that the kinks should have sufficient kinetic energy to overcome the pinning effects.

In Fig. 19, we plot the profiles $u(z)$ of the moving kinks that correspond to both two curves of Fig. 17. The profile in panel (a) corresponds to the moving kink from curve 1, whereas the profile in panel (b) to the kink from curve 2. In both the cases, the coupling constant was the same: $\kappa = 100$. The second kink appears to be wider and this can be explained by the fact that its velocity is more than two times smaller. The insets of the figures show the velocity profiles.

In Fig. 20, we investigate the behavior of moving kinks for different β 's. Increase of the barrier flatness is reflected in change of the shape at the kink center. We have considered the kinks corresponding to curve 2 of Fig. 18, when the coupling is fixed: $\kappa = 120$. Deformation of the kink profile can easily be seen on the velocity profile shown in the inset. The kink profile experiences deformation of its slope part, which is seen as a dip in the velocity profile. The dip grows with increase of β . More flat the barrier becomes, more possibilities of the kink's profile deformation.

These results demonstrate that the existence of a finite set of velocities, at which the kink can move with constant shape is a generic effect. Its appearance is due to the shape of the on-site (intrabond proton) potential. If the proton potential has a barrier which is flat enough to allow the symmetry switchings (accompanied by the pitchfork bifurcations), the Peierls-Nabarro barrier experiences lowering for specific values of the system parameters. Thus, it becomes possible that the kinetic energy of the kink is sufficient to overcome the pinning forces of the lattice.

VI. CONCLUSIONS

We have studied the dynamics of the one-dimensional Klein-Gordon lattice with the on-site potential of the double-Morse type. This is a physically motivated model, which is the simplest one for the proton transport in a hydrogen-bonded chain, where the on-site potential plays the role of the potential for proton transfers in the hydrogen bond. Therefore throughout this paper we call it an intrabond proton potential. A Morse-type function was found to offer the best combination of accuracy in reproducing quantum-mechanically computed poten-

tials [24,25]. The model has two parameters, the proton-proton coupling κ and the anharmonicity of the Morse potential, the curvature parameter β . The anharmonicity parameter is responsible for the shape of the intrabond potential $V(u)$, especially on the convexity of its barrier. For larger β , the barrier becomes more flat and the wells become more narrow. Changing this parameter, one can explore the variety of possible intrabond potentials, starting from the ϕ^4 model (as $\beta \rightarrow 0$) and finishing with the exactly solvable limit $\beta \rightarrow \infty$.

Deformation of the barrier of the intrabond potential becomes crucial for the properties of the stationary kink solutions. While the ϕ^4 limit allows us only *two* types of stationary kinks: ion-centered and proton-centered with their stability properties being constant for any coupling κ , the opposite limit shows the existence of an infinite countable set of stationary kink solutions. For some values of the coupling κ forming an infinite countable set, the states with different symmetries can have the same energy. In between these two limiting cases, some of the kink properties survive from the exactly solvable limit $\beta \rightarrow \infty$. First of all, the stability properties of the kink solutions depend drastically on the coupling parameter κ . With increase of κ , the initially stable ion-centered kink becomes unstable, while the proton-centered kink gets stable. With further increase of κ , these *stability switchings* which are, in fact, pitchfork bifurcations, go on several times. Another result can be seen for rather high β , at least, for $\beta > 20$, in our calculations. It is the coexistence of several kink solutions of the same symmetry for the same κ . This is a left-over from the exactly solvable limit and it disappears with lowering β . An analytical approximation has been constructed to show the effect of the symmetry switchings analytically and to confirm that the effect is not confined to a specific model, but has a universal nature.

The stability switchings contribute to the non-monotonic behavior of the Peierls-Nabarro (PN) barrier. The barrier decays with increase of κ , however, experiences local minima at the stability switching points, where its value decreases by one order of magnitude. The same happens for the dependence of the PN barrier on β . This phenomenon, in its turn, assists the kink mobility and leads to the appearance of a finite set of velocities for which the propagation of very *narrow* kinks is possible. This is a generic effect, attributed to the shape of the on-site (intrabond) potential, and also is not confined to a specific model. Note that the PN barrier is not required to vanish completely (see Ref. [20]). Simply, the barrier is low enough for the kinetic energy of the kink to carry it over the barrier.

Thus, we have concluded that highly mobile kinks are possible in our model of the proton transport in hydrogen-bonded chains even for those proton-proton nearest-neighbor interactions, when the proton kinks are very narrow. This gives us a reason to believe that the soliton mechanism of proton transfers can work for physically reasonable values of the proton-proton coupling κ .

This work has benefited from discussions with M. Peyrard. We acknowledge financial support from the RTN Project No. LOCNET HPRN-CT-1999-00163, the INTAS Grant No. 97-0368, and the Danish Research Agency.

-
- [1] For a review see, e.g., J. F. Nagle and S. Tristram-Nagle, *J. Membrane Biol.* **74**, 1 (1983).
 - [2] For details see, e.g., S. N. Vinogradov and R. H. Linnell, *Hydrogen Bonding* (Van Nostrand Reinhold Company, New York, 1971).
 - [3] C.-I. Chou, C.-L. Ho, B. Hu, and H. Lee, *Phys. Rev. E* **57**, 2747 (1998).
 - [4] See, e.g., the recent paper by A. V. Zolotaryuk, M. Peyrard, and K. H. Spatschek, *Phys. Rev. E* **62**, 5706 (2000), and references therein.
 - [5] Y. Kashimori, T. Kikuchi, and K. Nishimoto, *J. Chem. Phys.* **77**, 1904 (1982).
 - [6] St. Pnevmatikos, *Phys. Rev. Lett.* **60**, 1534 (1988).
 - [7] E. S. Kryachko, *Solid State Commun.* **65**, 1609 (1988); *Chem. Phys.* **143**, 359 (1990).
 - [8] E. S. Kryachko, M. Eckert, and G. Zundel, *J. Mol. Struct.* **235**, 157 (1991).
 - [9] St. Pnevmatikos, A. V. Savin, A. V. Zolotaryuk, Y. S. Kivshar, and M. J. Velgakis, *Phys. Rev. A* **43**, 5518 (1991).
 - [10] Y. P. Mei, J. R. Yan, X. H. Yan, and J. Q. You, *Phys. Rev. B* **48**, 577 (1993).
 - [11] Y. S. Kivshar, A. V. Savin, M. J. Velgakis, and A. V. Zolotaryuk, *Int. J. Mod. Phys. B* **8**, 1033 (1994).
 - [12] A. Godzik, *Chem. Phys. Lett.* **171**, 217 (1990).
 - [13] P. V. Hobbs, *Ice Physics* (Clarendon, Oxford, 1974).
 - [14] A. V. Savin and A. V. Zolotaryuk, *Phys. Rev. A* **44**, 8167 (1991).
 - [15] M. Peyrard and M. D. Kruskal, *Physica D* **14**, 88 (1984).
 - [16] O. M. Braun and Y. S. Kivshar, *Phys. Rep.* **306**, 2 (1998).
 - [17] M. Peyrard and M. Remoissenet, *Phys. Rev. B* **26**, 2886 (1982).
 - [18] A. V. Savin, Y. Zolotaryuk, and J. C. Eilbeck, *Physica D* **138**, 267 (2000).
 - [19] V. H. Schmidt, *Phys. Rev. B* **20**, 4397 (1979).
 - [20] S. Flach, Y. Zolotaryuk, and K. Kladko, *Phys. Rev. E* **59**, 6105 (1999).
 - [21] Y. Zolotaryuk, J. C. Eilbeck and A. V. Savin, *Physica D* **108**, 81 (1997).
 - [22] J. M. Speight, *Nonlinearity* **10**, 1615 (1997); **12**, 1373 (1999).
 - [23] N. J. Balmforth, R. V. Craster, and P. G. Kevrekidis, *Physica D* **135**, 212 (2000).
 - [24] X. Duan and S. Scheiner, *J. Mol. Struct.* **270**, 173 (1992).
 - [25] S. Scheiner and X. Duan, *ACS Symposium Series* **569**, 125 (1994).
 - [26] A. V. Zolotaryuk, St. Pnevmatikos, and A. V. Savin, *Physica D* **51**, 407 (1991).
 - [27] R. Grauer, K. H. Spatschek, and A. V. Zolotaryuk, *Phys.*

- Rev. E **47**, 236 (1993).
- [28] M. H. Jensen, P. Bak, and A. Popielewicz, J. Phys. A: Math. Gen. **16**, 4369 (1983).
 - [29] J. L. Marín, F. Falo, and P. J. Martínez, and L. M. Flórida, Phys. Rev. E **63**, 066603 (2001).
 - [30] J. H. Weiner and A. Askar, Nature **226**, 842 (1970).
 - [31] S. F. Mingaleev, Y. B. Gaididei, E. Majernikova, and S. Shpyrko, Phys. Rev. E **61**, 4454 (2000).
 - [32] O. M. Braun, Y. Kivshar, and M. Peyrard, Phys. Rev. E **56**, 6050 (1997).
 - [33] J. C. Eilbeck and R. Flesch, Phys. Lett. A **149**, 200 (1990); D. B. Duncan, J. C. Eilbeck, H. Feddersen, and J. A. D. Wattis, Physica D **68**, 1 (1993).

FIG. 1. Schematics of interactions in the hydrogen bond.

FIG. 2. The shape of the intrabond potential $V(u)$ given by Eq. (6) with $a = 0.25$ for $\beta = 5$ (curve 1), $\beta = 20$ (curve 2), and $\beta = 50$ (curve 3).

FIG. 3. Profiles of monotonic symmetric kinks with $\beta = 5$ and $\kappa = 30$: (a) ion-centered kink and (b) proton-centered kink.

FIG. 4. Dependence of the kink energy E_m , $m = 0, 1, 2, 3$, and 4, given by Eq. (18), in the exactly solvable limit $\beta \rightarrow \infty$ on the coupling parameter κ .

FIG. 5. Dependence of energy for $\beta=10$ on coupling κ for symmetric ion-centered kink (curve 1), symmetric proton-centered kink (curve 2), and zigzag-like kinks (curves 4 and 5). The inset shows more detailed behavior in the vicinity of stability switchings and curve 3 corresponds to the kink with asymmetric profile. Solid lines correspond to stable states and dashed lines to unstable ones.

FIG. 6. Profiles of monotonic asymmetric kinks with $\beta = 10$ and $\kappa = 24$. Inversion of these profiles is clearly seen from comparison of panels (a) and (b).

FIG. 7. Zigzag-like kink profiles for $\beta = 10$ and $\kappa = 8$: (a) ion-centered and (b) proton-centered kinks.

FIG. 8. Dependence of the displacement of the central particle from equilibrium (at $u_{N/2} = 0$) on the coupling κ for proton-centered (curve 1), ion-centered (curves 2 and 3), and asymmetric (curve 3) kinks with $\beta=10$. Solid lines show stable kinks and dashed lines unstable ones.

FIG. 9. Dependence of the kink energy for $\beta=20$ on the coupling κ (see text for details). The solid line shows stable states and the dashed lines unstable ones.

FIG. 10. Kink solutions corresponding to curves 1 (o) and 4 (+) of Fig. 9 for $\kappa = 25$.

FIG. 11. Schematic representation of the approximate potential (20).

FIG. 12. Dependence of the system eigenfrequencies Ω_n on the coupling parameter κ for $\beta = 5$: (a) ion-centered and (b) proton-centered kinks and for $\beta = 10$: (c) ion-centered and (d) proton-centered kinks. Curves depicted by small dots correspond to cases, when Ω_n 's are purely imaginary and therefore $\text{Im } \Omega_n$'s are plotted instead (see text for details).

FIG. 13. Example of eigenvectors for the case with $\beta = 10$ and $\kappa = 10$. For the ion-centered kink: (a) the eigenvector of the lowest localized mode and (b) the eigenvector of the first excited localized mode. For the proton-centered kink: the eigenvectors of (c) the lowest, (d) the first, and (e) the second localized modes.

FIG. 14. Example of eigenvectors for $\beta = 10$ and $\kappa = 30$: (a), (b), (c), and (d) - eigenvectors of the localized modes for the ion-centered kink from the lowest to the highest mode; (e), (f), and (g) - the same for the proton-centered kink.

FIG. 15. Peierls-Nabarro potential for $\beta = 10$ and (a) $\kappa = 70.5$, (b) $\kappa = 71.22$, (c) $\kappa = 71.288$, (d) $\kappa = 71.35$, and (e) $\kappa = 72$.

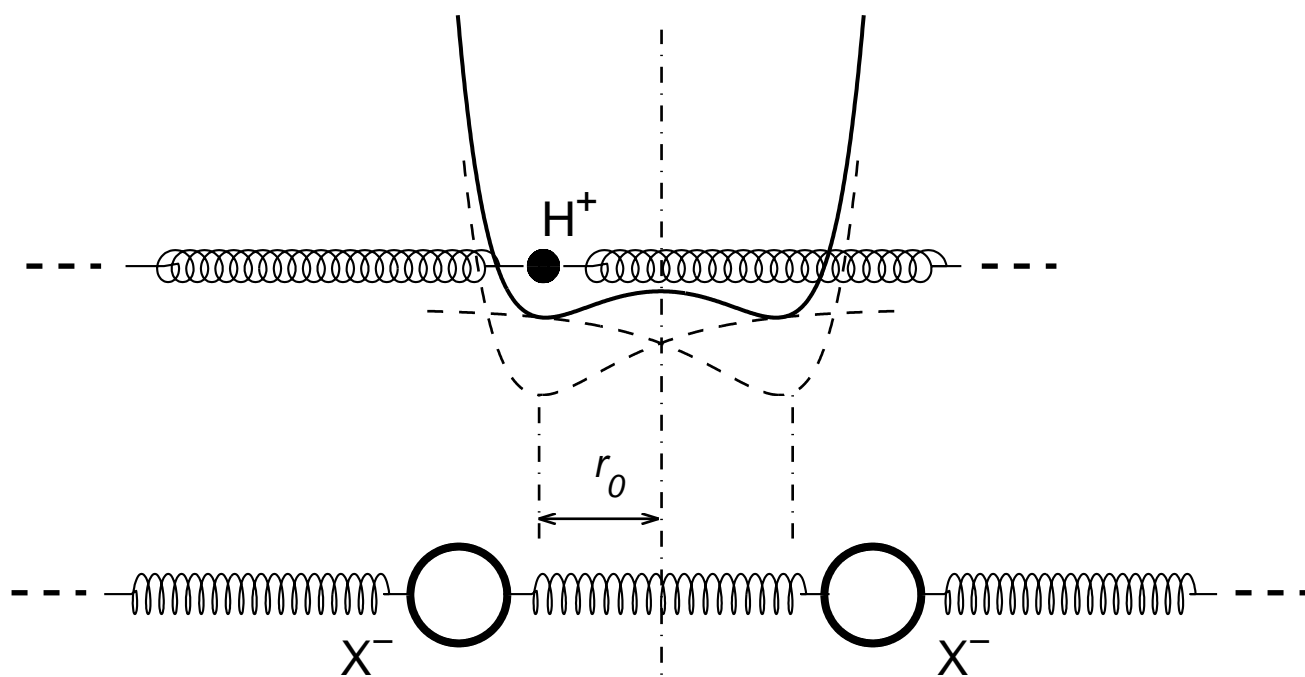
FIG. 16. Dependence of the height of the PN barrier on the parameter β for $\kappa = 30$. The upper inset shows the shape of the PN barrier before the minimum at $\beta = 7.8$ (curve 1) and after the minimum at $\beta = 8.8$ (curve 2). The lower inset shows more detailed behavior of δE around its minimum.

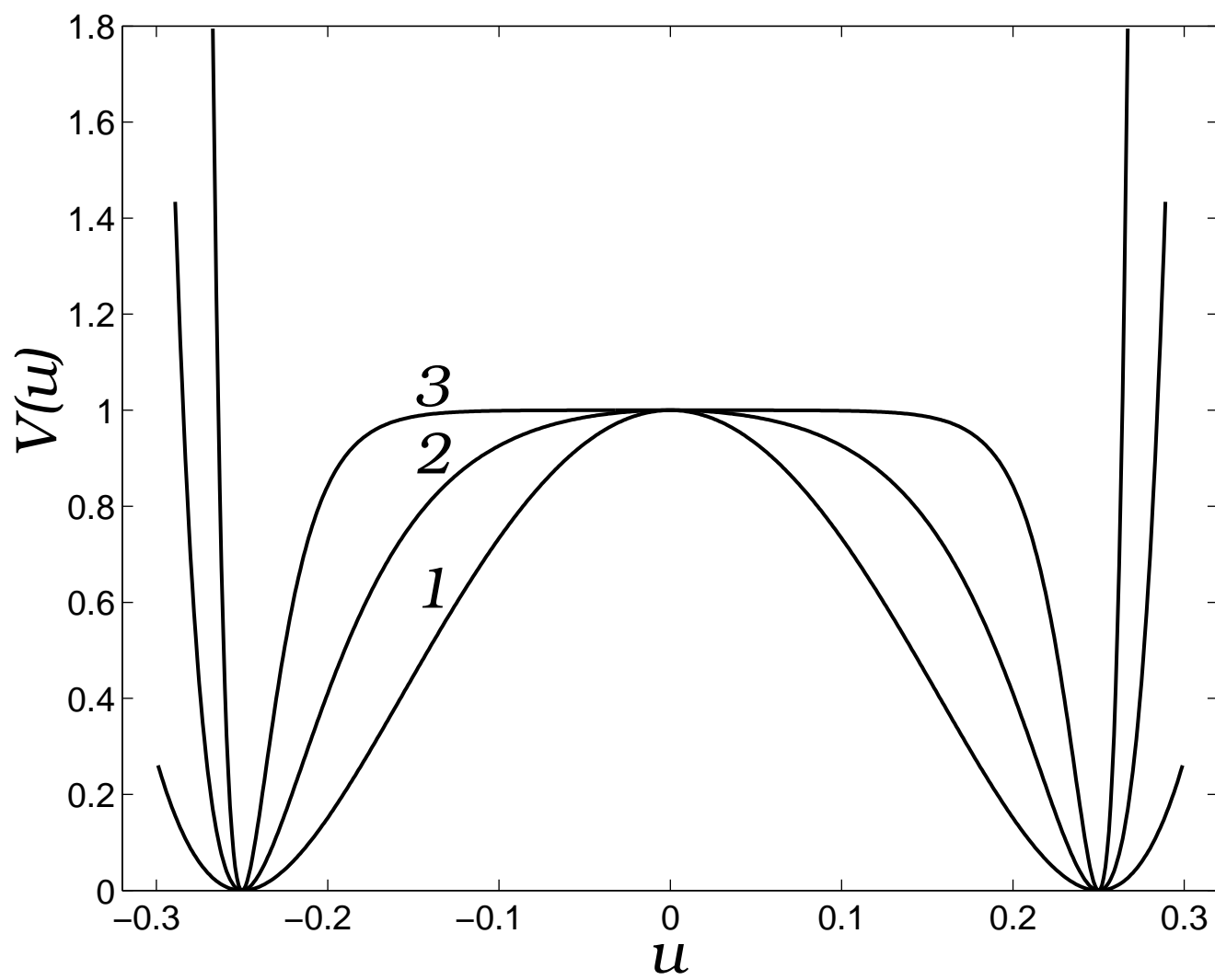
FIG. 17. Normalized velocity of the non-oscillating kink motion against the coupling parameter κ for $\beta = 10$.

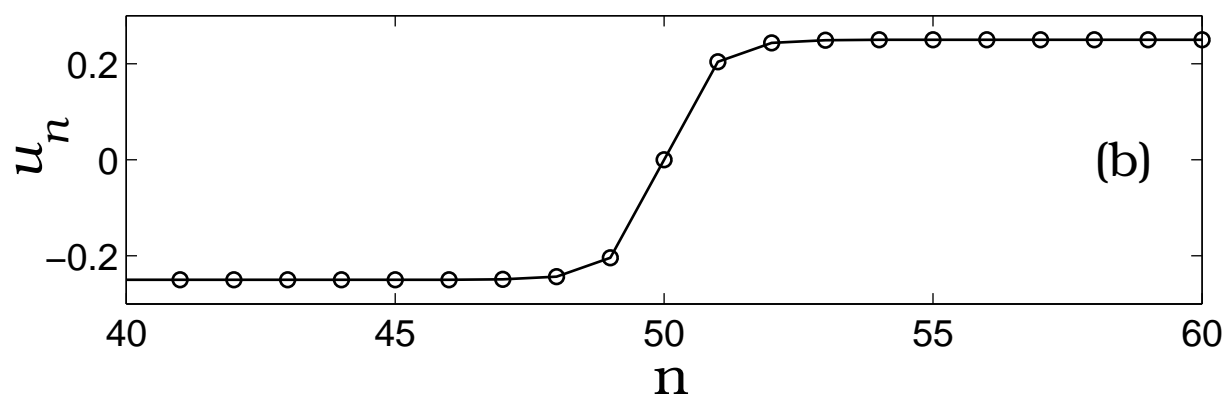
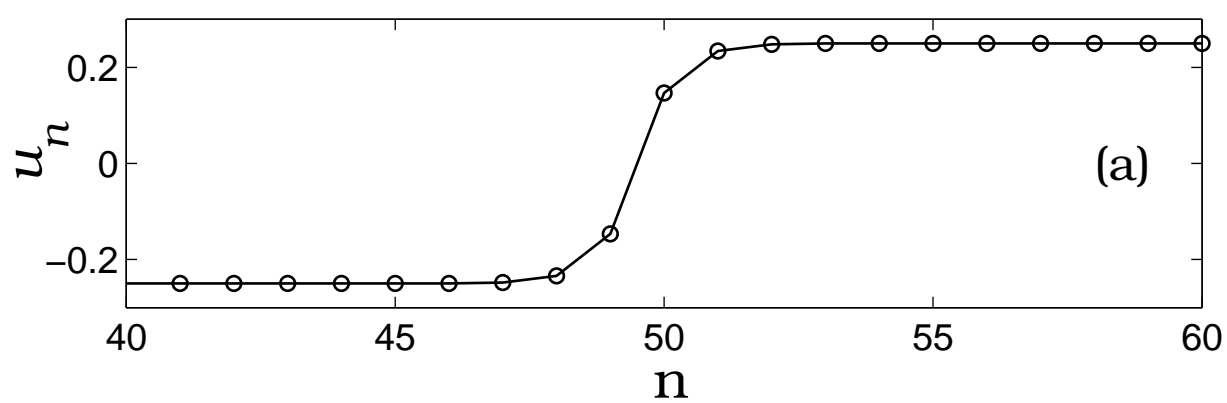
FIG. 18. Normalized velocity of the non-oscillating kink motion against parameter β for $\kappa = 120$.

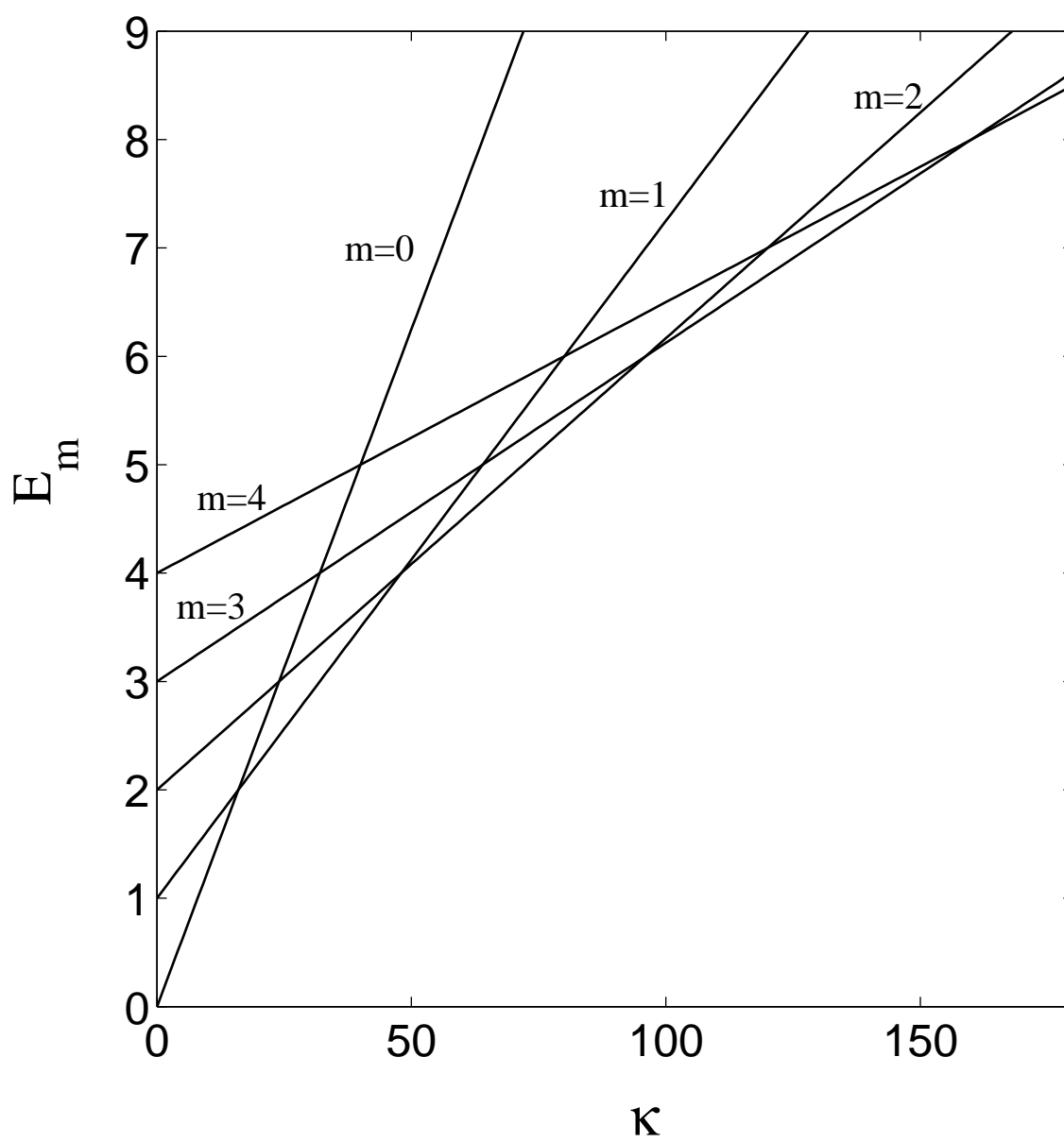
FIG. 19. Examples of moving antikinks at $\beta = 10$ and $\kappa = 100$ with velocities: (a) $s = 6.227$ and (b) $s = 2.463$. Circles show positions of lattice sites.

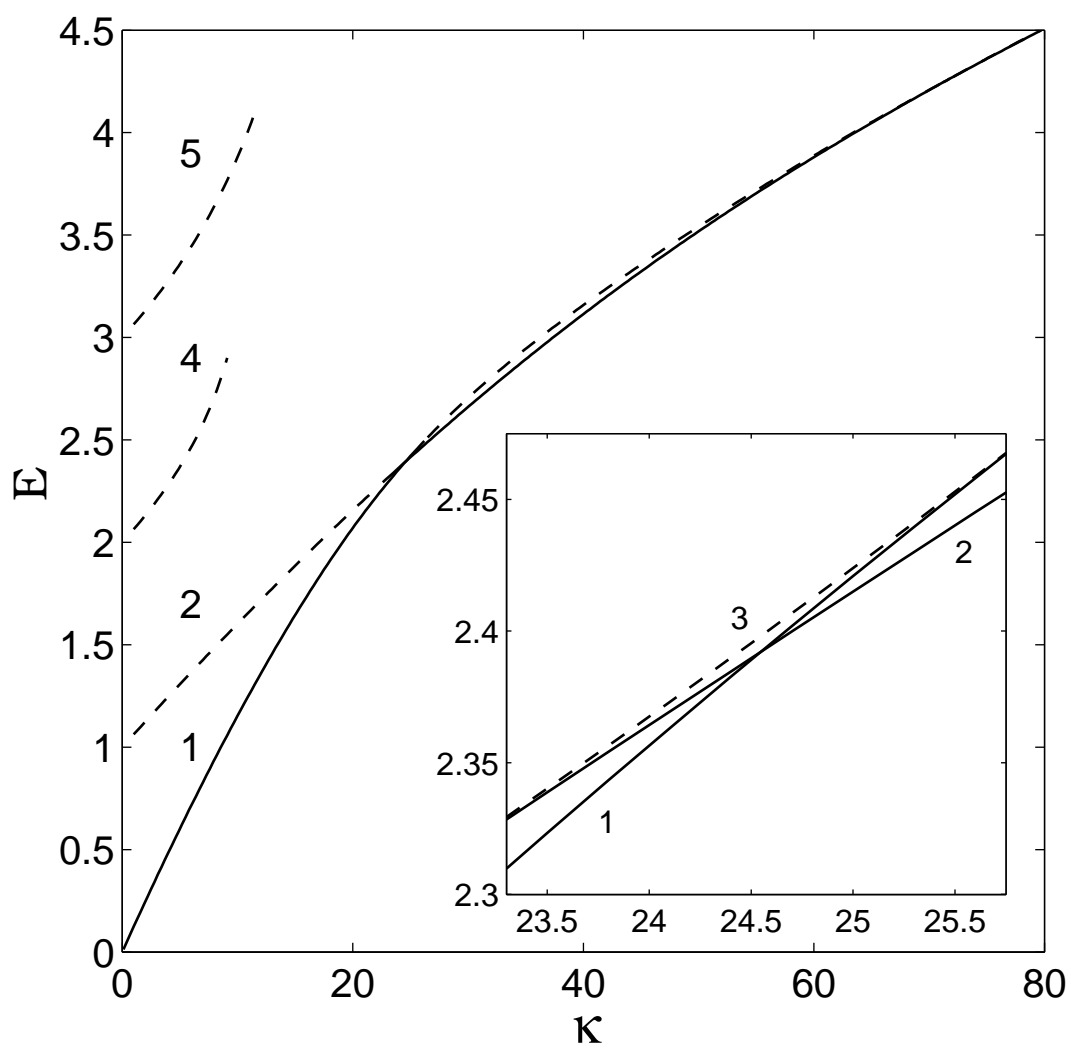
FIG. 20. Examples of moving antikinks at $\kappa = 120$: (a) $\beta = 12$ and $s = 4.154$, (b) $\beta = 15$ and $s = 4.551$, (c) $\beta = 20$ and $s = 4.734$. Circles show positions of lattice sites.

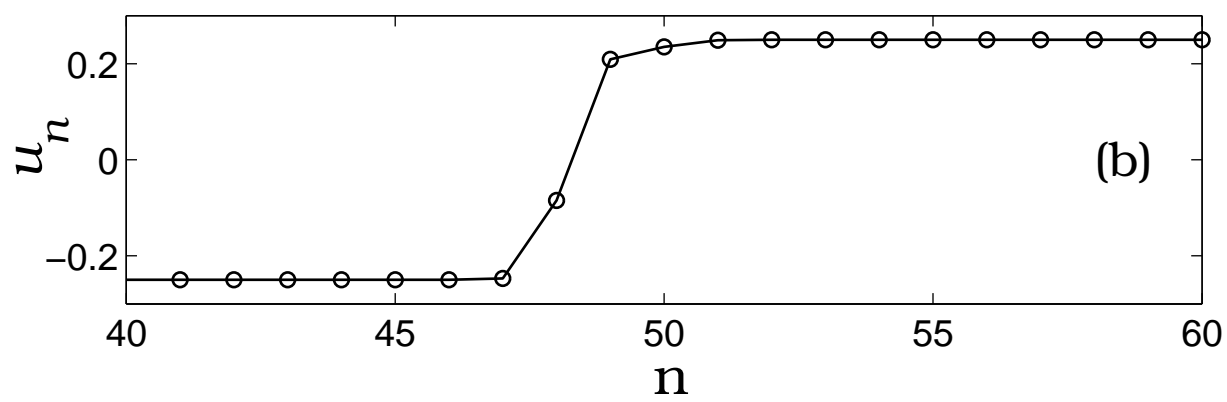
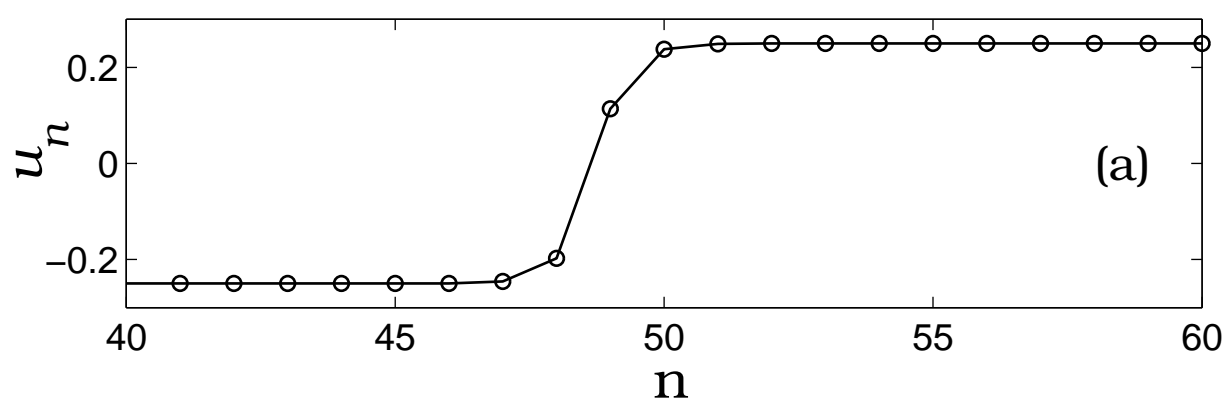


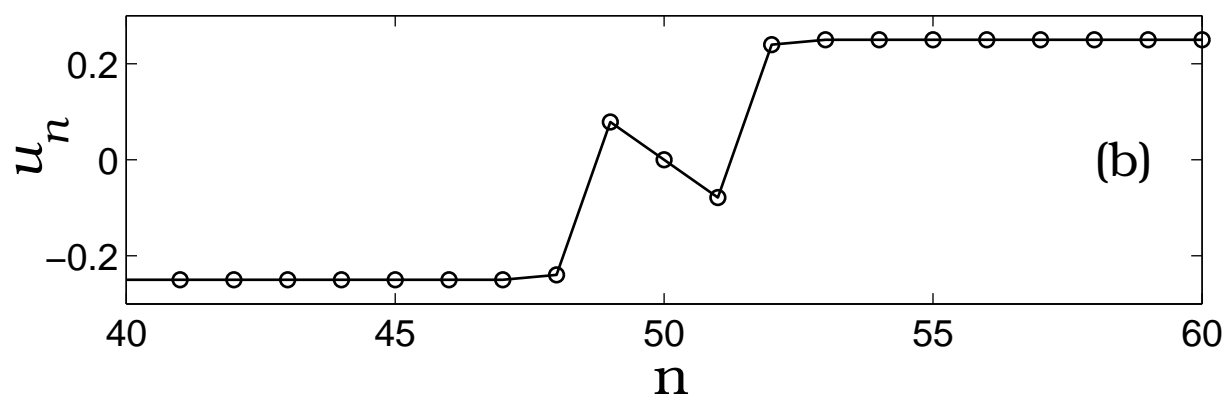
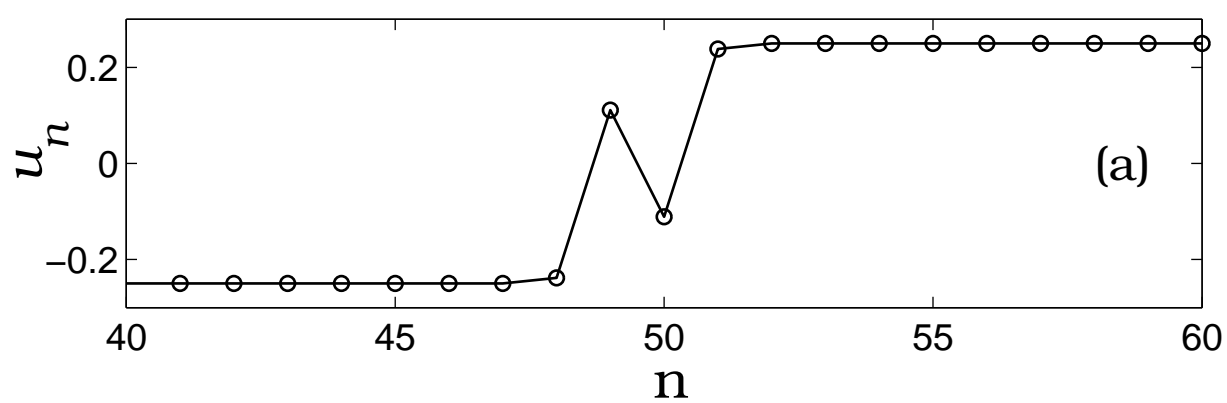


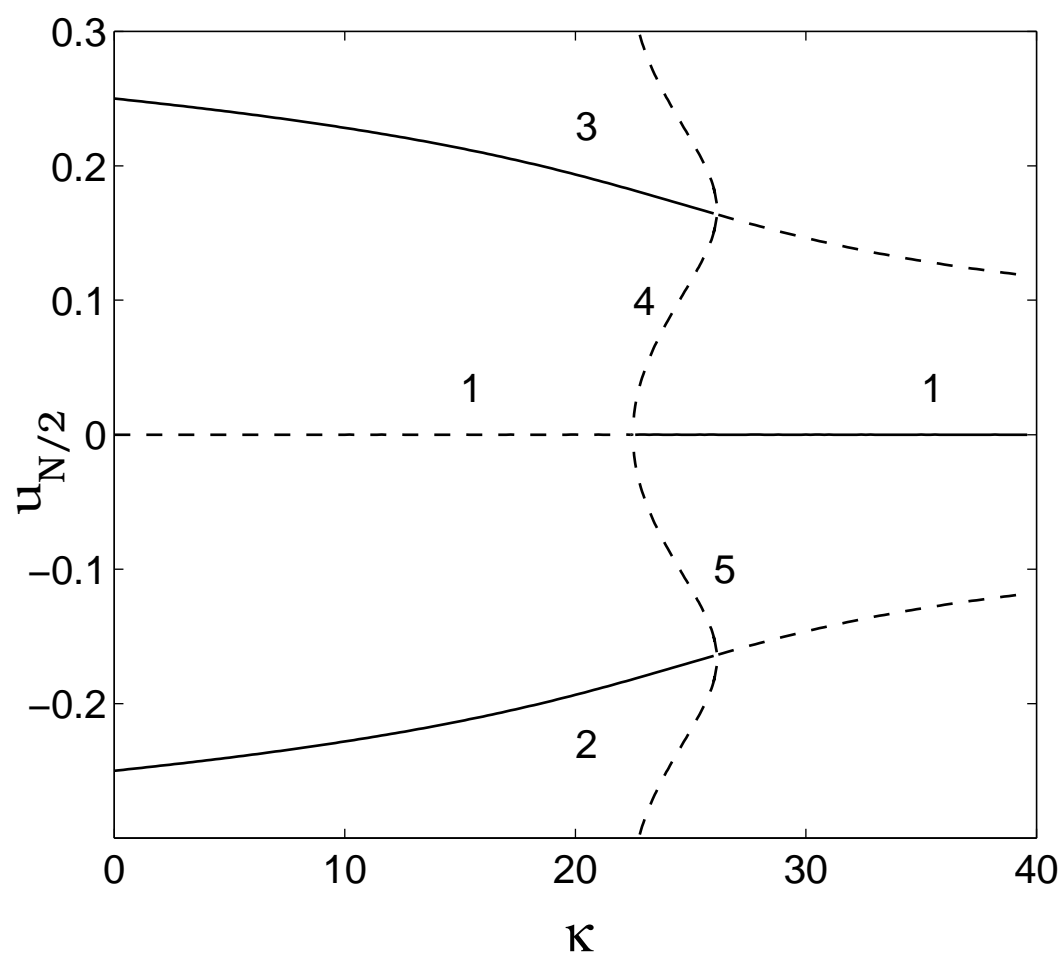


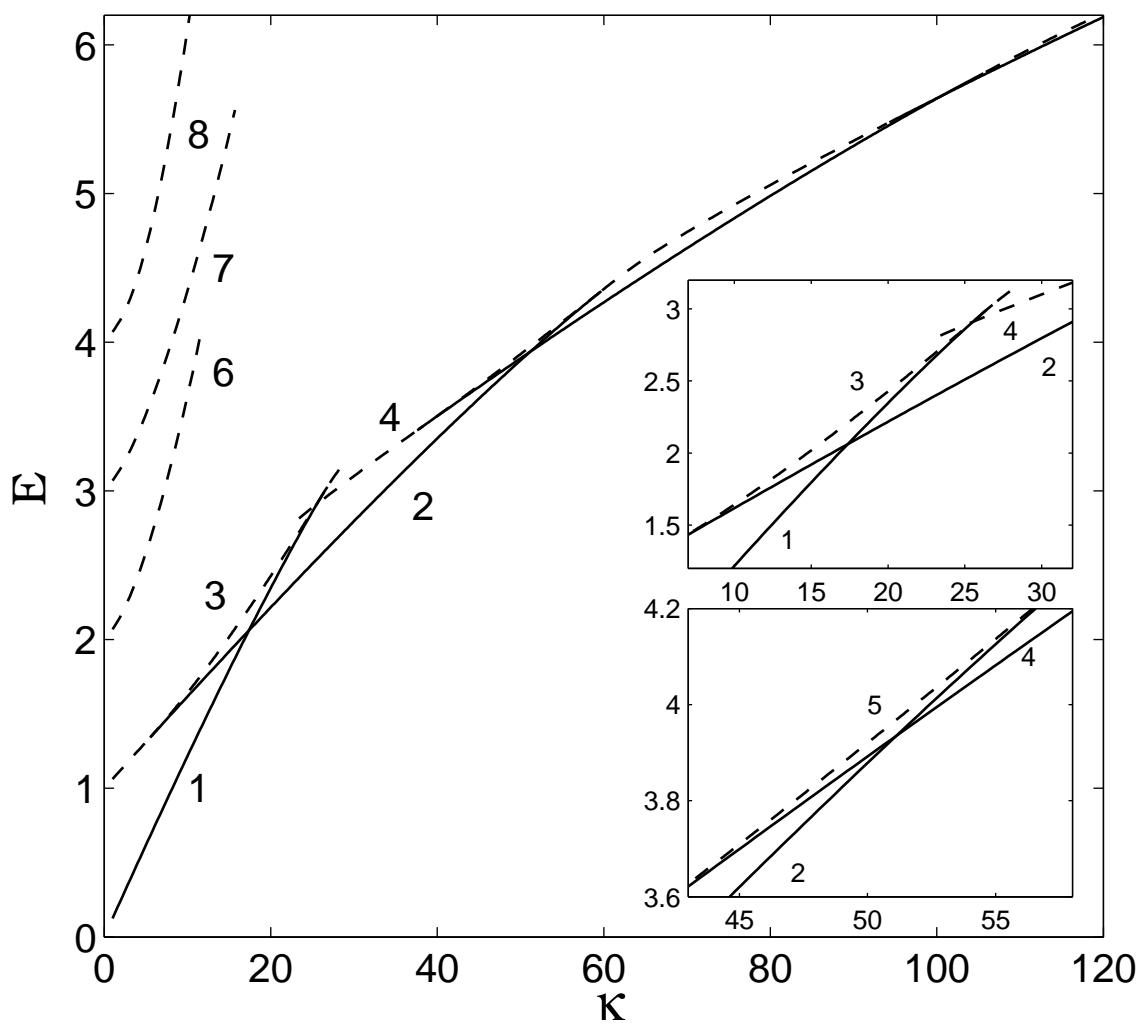


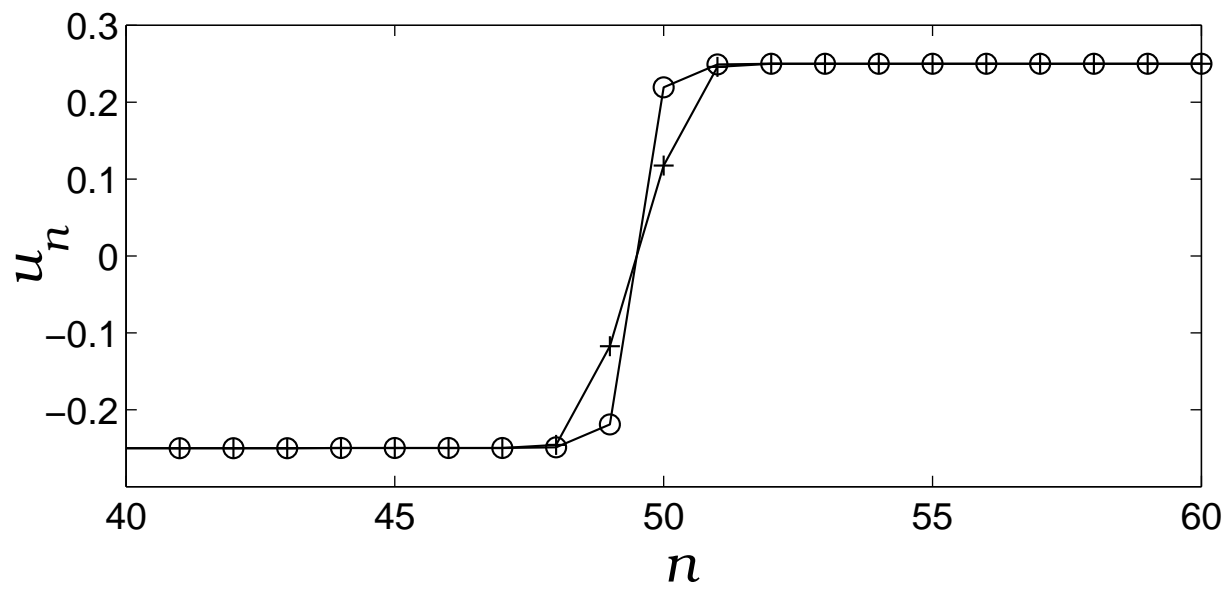


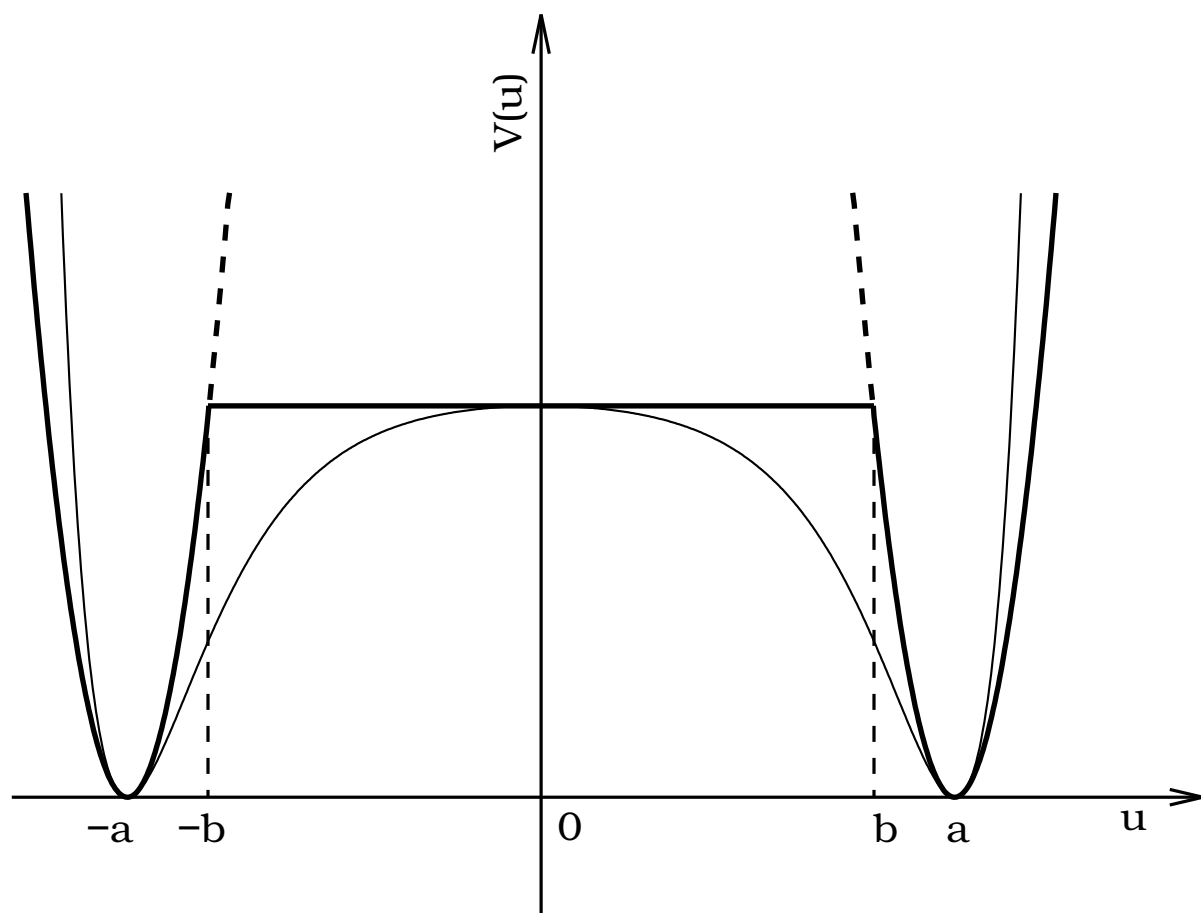












This figure "fig12.gif" is available in "gif" format from:

<http://arxiv.org/ps/nlin/0208049v1>

